JACS
JOURNAL OF THE AMERICAN CHEMICAL SOCIETY

ARTICLE

pubs.acs.org/JACS

The Need for Enzymatic Steering in Abietic Acid Biosynthesis: Gas-Phase Chemical Dynamics Simulations of Carbocation Rearrangements on a Bifurcating Potential Energy Surface

Matthew R. Siebert,[†] Jiaxu Zhang,[†] Srirangam V. Addepalli,[‡,#] Dean J. Tantillo,[§] and William L. Hase*[,†]

[†]Department of Chemistry and Biochemistry and [‡]High Performance Computing Center, Texas Tech University, Lubbock, Texas 79409, United States

[§]Department of Chemistry, University of California—Davis, Davis, California 95616, United States

Supporting Information

ABSTRACT: Abietic acid, a constituent of pine resin, is naturally derived from abietadiene — a process that requires four enzymes: one (abietadiene synthase) for conversion of the acyclic, achiral geranylgeranyl diphosphate to the polycyclic, chiral abietadiene (a complex process involving the copalyl diphosphate intermediate) and then three to oxidize a single methyl group of abietadiene to the corresponding carboxylic acid. In previous work (*Nature Chem.* **2009**, *1*, 384), electronic structure calculations on carbocation rearrangements leading to abietadienyl cation revealed an interesting potential energy surface with a bifurcating reaction pathway (two transition-state structures connected directly with no intervening minimum), which links two products — one natural and one not yet isolated from Nature. Herein we describe direct dynamics simulations of the key step in the formation of abietadiene (in the gas phase and in the absence of the enzyme). The simulations reveal that abietadiene synthase must intervene in order to produce abietadiene selectively, in essence steering this reaction to avoid the generation of byproducts with different molecular architectures.

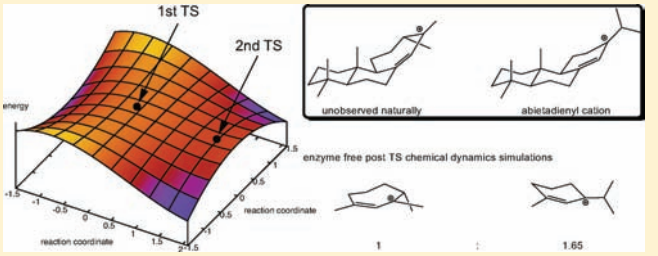

INTRODUCTION

Some evergreens, including the grand fir (*Abies grandis*), possess a great defense against physical injury: when wounded they secrete tall oil, also known as pine resin. Pine resin is a complex mixture of mono- (C_{10}), sesqui- (C_{15}), and diterpenoids (C_{20}).[1] The low-molecular-weight mono- and sesquiterpenoids act as toxins to insects that may attack the grand fir, such as Bark beetles and their symbiots; further they act as solvent to mobilize diterpenoids to the wound site.[1] Once there, volatilization of the mono- and sesquiterpenoids results in concentration and oxidative polymerization of the diterpenoids, effectively sealing wounds and preventing further damage to the majestic trees.[1] Tall oil is not only of use to *Abies grandis*; it is also collected as a byproduct of the paper industry (although some companies harvest it from living trees) and is traded on the global market mainly for one constituent: rosin.[2] Rosin, which makes up one-quarter of tall oil, finds use in many products including inks, adhesives, paper sizing, and chewing gum base.[2]

Abietic acid is the diterpenoid present in tall oil mainly responsible for its polymerizable nature.[1] It is naturally derived from geranylgeranyl diphosphate through the pathway depicted in Scheme 1.[3] Geranylgeranyl diphosphate is first transformed by abietadiene synthase[3a−d] to abietadiene. Next, oxidation of the C18 methyl group[4] is carried out in a process that involves two different cytochrome P450s (mono-oxygenases) and one dehydrogenase enzyme.[3e]

Terpene cyclase enzymes (including abietadiene synthase)[3,5,6] have enjoyed a generous amount of attention, in part due to the efficiency of the cyclization procedures that take acyclic precursors to complex, polycyclic ring structures.[5] Experiments have shown that abietadiene synthase first converts geranylgeranyl diphosphate to copalyl diphosphate before passive diffusion to a second active site occurs, where the newly formed copalyl diphosphate is converted to abietadiene (see Scheme 1).[3d] It has also been shown that conversion of copalyl diphosphate to abietadiene occurs in a multistep process and involves the pimaradienyl cation intermediate, as depicted in Scheme 2.[3f−i]

In 2009, electronic structure calculations showed that the proton and methyl shifts (blue and red arrows, Scheme 2) can occur in a concerted but very asynchronous fashion.[5i,7] Of even greater importance, the calculations indicate the presence of a potential energy surface (PES) with a bifurcation[8] to form two products during the concerted/asynchronous conversion of pimaradienyl cation to abietadienyl cation. This is illustrated with more detail in Scheme 3 for a truncated system that has been shown to behave similarly.[5i]

PES bifurcations (see Figure 1 for a generic example) are characterized by two consecutive transition states (TSs) with no intervening minimum.[9] Reports of such topological features are

Received: March 9, 2011
Published: May 06, 2011

ACS Publications © 2011 American Chemical Society

Scheme 1. Biosynthetic Formation of Abietic Acid from Geranylgeranyl Diphosphate[3,4]

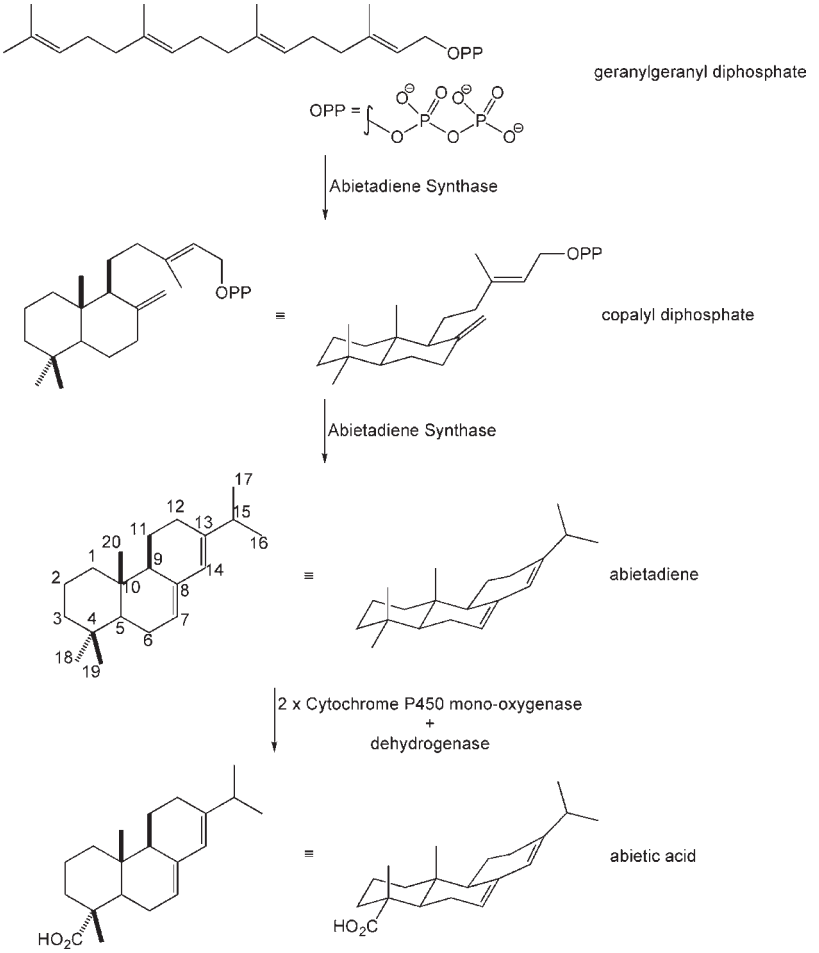

Scheme 2. Mechanism for conversion of copalyl diphosphate to abietadiene

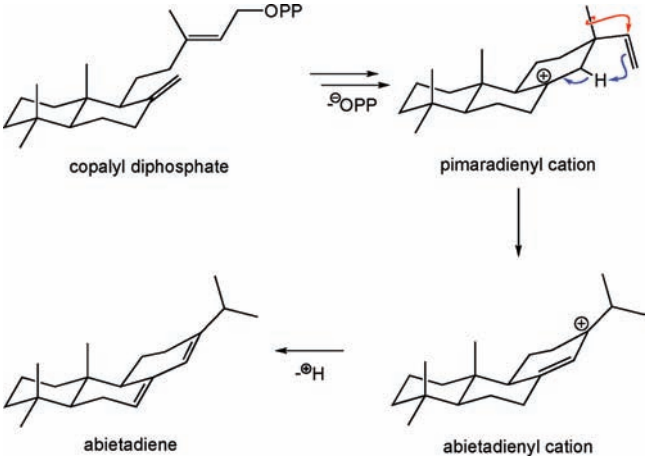

Scheme 3. Details of a PES Bifurcation Leading to Either of Two Products: 4 (an Analogue of Abietadienyl Cation) and 5 (an Analogue of a Heretofore Unobserved Product)[a]

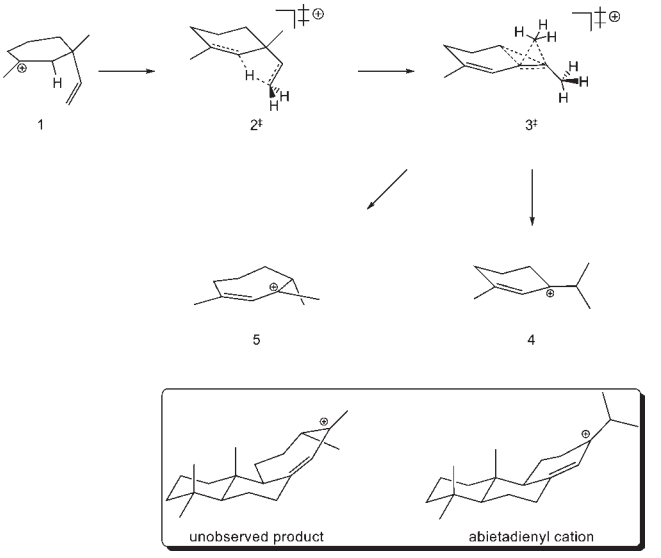

[a] Full C_{20} congeners of the two products appear directly below their truncated forms.

appearing more frequently, although the bulk of the chemical systems involved are very small (under 10 non-hydrogen atoms), and often these bifurcations link indistinguishable (symmetry-related) isomers.[8] An increasingly large number of reaction pathways have been shown to bifurcate to chemically unique

dx.doi.org/10.1021/ja201730y |J. Am. Chem. Soc. 2011, 133, 8335–8343

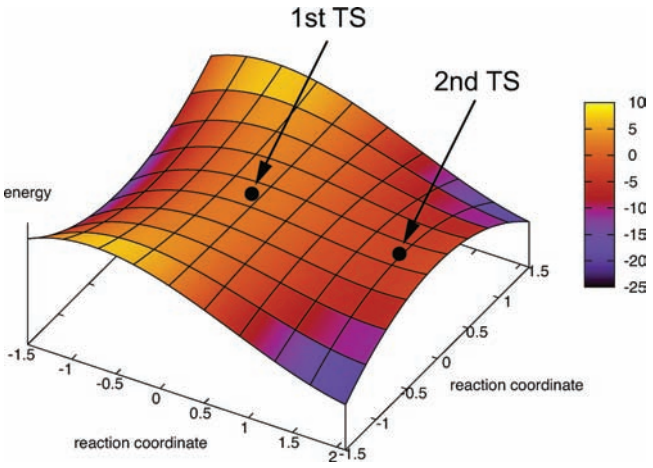

Figure 1. Generic example of a PES exhibiting a bifurcating pathway.[12] Surface details: $f(x,y) = 2x^3 - 5x^2 - 5xy^2 + y^2 + 2$; saddle points are located at (0,0,2) and (1.67,0, −2.63).

products.[8] The bifurcation described in Scheme 3 falls into this category, in which products with dramatically different chemical scaffolds are formed. Furthermore, to the best of our knowledge this case appears to be the first involving a biologically relevant PES bifurcation. It is generally recognized that accurate prediction of product distributions for such systems is obtainable only through chemical dynamics simulations.[8,10,11]

Herein, we report a gas-phase (enzyme-free) post-transition state[10] direct dynamics[13] simulation of TS $\mathbf{2}^{\ddagger}$ shown in Scheme 3. Our aim is to determine if, in the absence of an enzyme, there is an inherent preference for the naturally occurring product as a result of chemical dynamics effects. Comparison of our chemical dynamics simulation data to the natural (enzyme-catalyzed) process reveals whether an appreciable amount of the unobserved product (**5**) would be formed in the absence of the enzyme, and therefore whether the enzyme must steer the chemical reaction.

COMPUTATIONAL METHODS

Electronic Structure Calculations and Model for the PES. Electronic structure calculations were performed with the NWChem[14] computer program to establish the level of theory needed to represent the PES for the post-transition-state dynamics of TS $\mathbf{2}^{\ddagger}$. Geometry optimizations of stationary points were performed using the MP2,[15] B3LYP,[16] BB1K,[17] and M05-2X[18] electronic structure theories paired with the 6-31+G(d,p)[19] basis set. The aug-cc-pVDZ[20] basis set was paired with each of the above models in test calculations; however, all proved cost-prohibitive except for B3LYP. These model theories were recently evaluated for their efficacy in describing the energetics of several reactions, including reactions involving transfer of hydrogen and heavy atoms.[21] Stationary points were classified as minima or TS structures by frequency analysis. Energies reported for computed stationary points are electronic energies (E) with unscaled zero-point energy (ZPE) corrections. CCSD(T)[22]/aug-cc-pVDZ[20] single-point (energy) calculations were carried out to benchmark the energy of each stationary point, and the energies reported from this level include ZPE corrections (unscaled) from the underlying (lower level) method.

The previous electronic structure calculations by Hong and Tantillo[5i] for the PES utilized the B3LYP functional, a hybrid density functional theory (DFT) method that has been extensively questioned for some of its shortcomings, which include troubles with describing extended π-systems[23] and van der Waals interactions,[24] along with a reported size dependence[25] and a failure to describe 1,3-alkyl-alkyl interactions,[26] among other things.[27] To evaluate any error in the B3LYP method, stationary points for the PES were fully optimized with two other DFT methods, BB1K[17] and M05-2X,[18] as well as the wave function theory (WFT)-based MP2[15] method, and the calculated energies are listed and compared in Table 1.

As is evident from the relative energies displayed in Table 1, all the stationary points were found at all levels of theory, with exception of TS $\mathbf{3}^{\ddagger}$ with M05-2X, which remained elusive despite repeated attempts to locate it. It is possible that the TS could be found by using different TS searching algorithms. It is important to note that the relative energies displayed in Table 1 are, in general, very similar across all the various methods. Comparing DFT- and WFT-based approaches is easiest for B3LYP and MP2. For neutral, closed-shell molecules, it is believed that MP2 generally overestimates barriers while B3LYP underestimates them.[28] It has been noted in previous studies that MP2 favors delocalized structures in cationic molecules,[29] which explains the observed discrepancy in energetics and structures (see Supporting Information for optimized coordinates).

To more accurately quantify the differences between B3LYP and MP2 optimized geometries, CCSD(T) single-point energy calculations were carried out, and the results appear in Table 1. Of note is that

Table 1. Relative Energies ($\Delta E + \Delta$ZPE in kcal/mol) for Stationary Points 2−5 (Relative to 1) and Relative Cost As Computed with B3LYP, BB1K, M05-2X, MP2, and CCSD(T)

entry	method[a]	$\mathbf{2}^{\ddagger}$	$\mathbf{3}^{\ddagger}$	**4**	**5**	cost[b]
1	B3LYP/6-31+G(d,p) (Gaussian03)[c]	26.08	7.33	−27.44	−19.51	–
2	B3LYP/6-31+G(d,p)	26.06	7.55	−27.43	−19.50	1.00
3	B3LYP/aug-cc-pVDZ	25.37	7.90	−26.65	−18.28	14.81
4	BB1K/6-31+G(d,p)	26.64	9.13	−25.51	−16.89	2.61
5	M05-2X/6-31+G(d,p)	27.01	[d]	−23.94	−13.48	2.57[e]
6	MP2/6-31+G(d,p)	25.50	8.94	−23.54	−14.76	8.05
7	CCSD(T)/6-31+G(d,p)//B3LYP/6-31+G(d,p)[f]	29.58	9.24	−22.86	−14.46	–
8	CCSD(T)/aug-cc-pVDZ//B3LYP/6-31+G(d,p)[f]	26.98	10.25	−20.57	−12.69	–
9	CCSD(T)/6-31+G(d,p)//MP2/6-31+G(d,p)[f]	29.06	9.16	−22.51	−14.13	–
10	CCSD(T)/aug-cc-pVDZ//MP2/6-31+G(d,p)[f]	26.41	10.27	−19.89	−12.18	–

[a] All calculations carried out herein were completed using NWChem. [b] Cost is defined as the average amount of CPU time to carry out a frequency calculation for a given method divided by that for B3LYP/6-31+G(d,p) (NWChem). [c] Values from ref 5i. [d] Transition structure $\mathbf{3}^{\ddagger}$ could not be located with M05-2X, despite multiple attempts. [e] Relative cost considers everything except $\mathbf{3}^{\ddagger}$. [f] Single-point energies computed with coupled cluster include ZPE corrections (unscaled) from the underlying (lower level) geometry optimization.

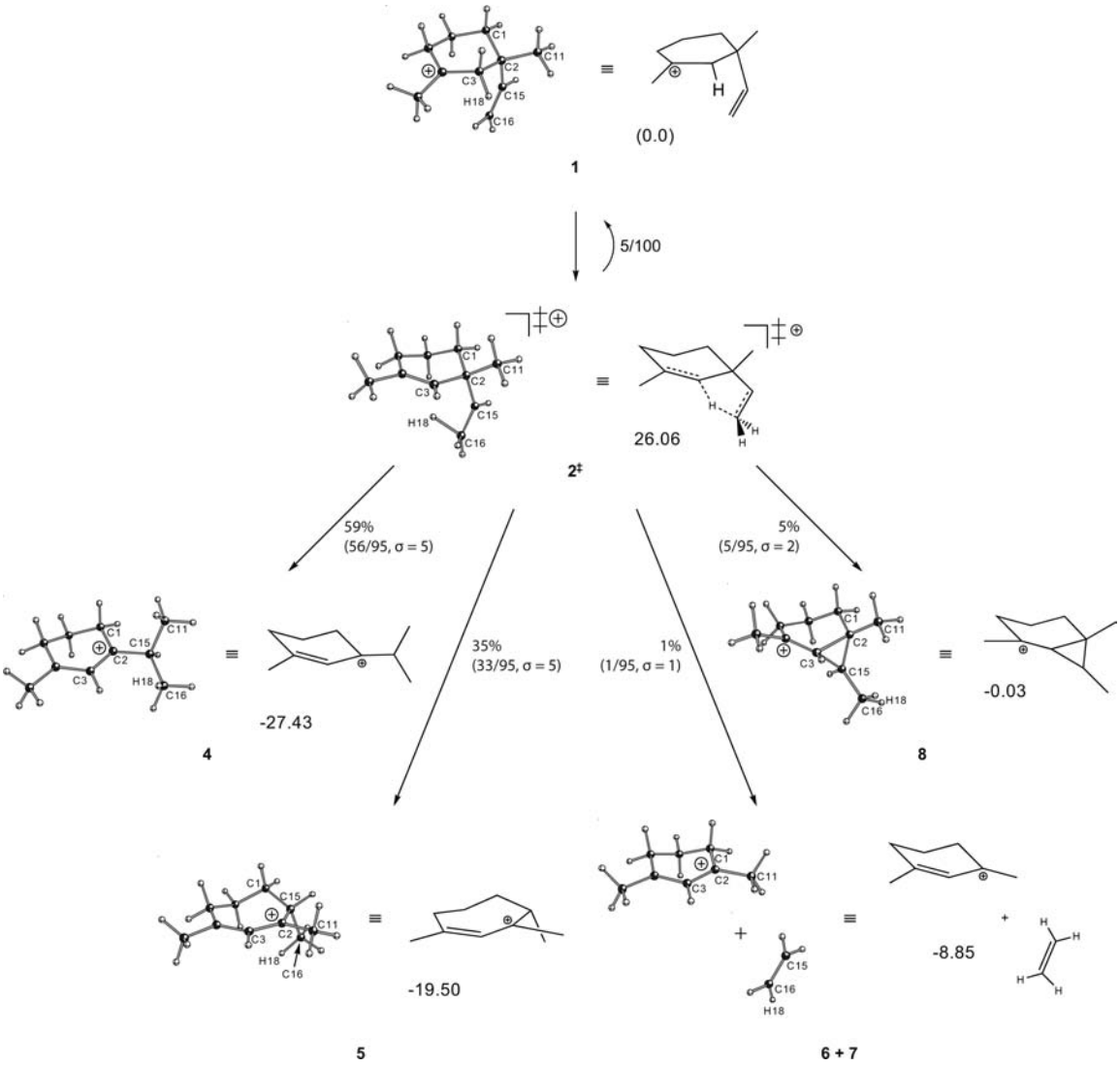

Figure 2. Summary of results from 100 velocity Verlet trajectories utilizing 0.5 fs time steps and B3LYP/6-31+G(d,p) forces. Five out of the 100 total trajectories recross the TS and form reactant **1**. The percentages of the reactive trajectories (95 in total) are normalized to add to 100%.

CCSD(T) requires a slightly larger basis set to accurately determine the energies, as evidenced by relatively large differences in energy on going from the 6-31+G(d,p) basis set to the slightly larger aug-cc-pVDZ (compare, e.g., entries 7 and 8). The CCSD(T)/aug-cc-pVDZ single-point calculations reveal that in this system B3LYP/6-31+G(d,p) more accurately determines the structure of minima than does MP2/6-31+G(d,p), as evidenced by lower energies for minima **4** and **5** when comparing entries 8 and 10.

The relative cost, defined as the average amount of CPU time to carry out a frequency calculation for a given method divided by that for B3LYP/6-31+G(d,p) (NWChem), is also displayed in Table 1. B3LYP/6-31+G(d,p) is the most computationally efficient and also provides a semiquantitative representation of the PES. It is the method used for most of the direct dynamics trajectories reported here. A smaller number of trajectories were calculated using the MP2/6-31+G(d,p) PES.

Although energetic criteria are important, we are interested in the evolution of dynamics across the PES, so nonlocal properties are also of importance; i.e., what are the differences in *shape* of the PESs for the different electronic structure methods? Vibrational frequency analyses provide this type of information (see Supporting Information for the imaginary frequencies (λ) for TSs $\mathbf{2}^{\ddagger}$ and $\mathbf{3}^{\ddagger}$). Overall, the imaginary frequencies for the different DFT methods, with the 6-31+G(d,p) basis set, are all very similar, providing additional support for the use of B3LYP for the direct dynamics as compared to either of the other two DFT methods that are substantially more computationally expensive. For TS $\mathbf{2}^{\ddagger}$, DFT λ values (in cm^{-1}) vary from 1296i to 1351i, while the MP2 value is 1203i. For TS $\mathbf{3}^{\ddagger}$, DFT λ values vary from 94i to 118i, and the MP2 value is 125i.

Computational Details of the Direct Dynamics Simulations. *Integrating the Classical Equations of Motion.* The B3LYP/6-31+G(d,p) direct dynamics simulations were performed with VENUS05,[30] coupled to NWChem. To perform the direct dynamics it is important to have an efficient method for accurately integrating Newton's equation of motion. This was established by calculating a sample trajectory with the velocity Verlet,[31] sixth-order symplectic,[32] and Hessian[33] integrators and with variation in the integration time step for the former two methods and variation in the trust radius for the latter. Although the sixth-order symplectic integrator provided the least variation in relative energy, its computational cost is excessive. The velocity Verlet integrator, with a 0.5 fs time step, was taken as a reasonable compromise between accuracy and computational time. The computational time for

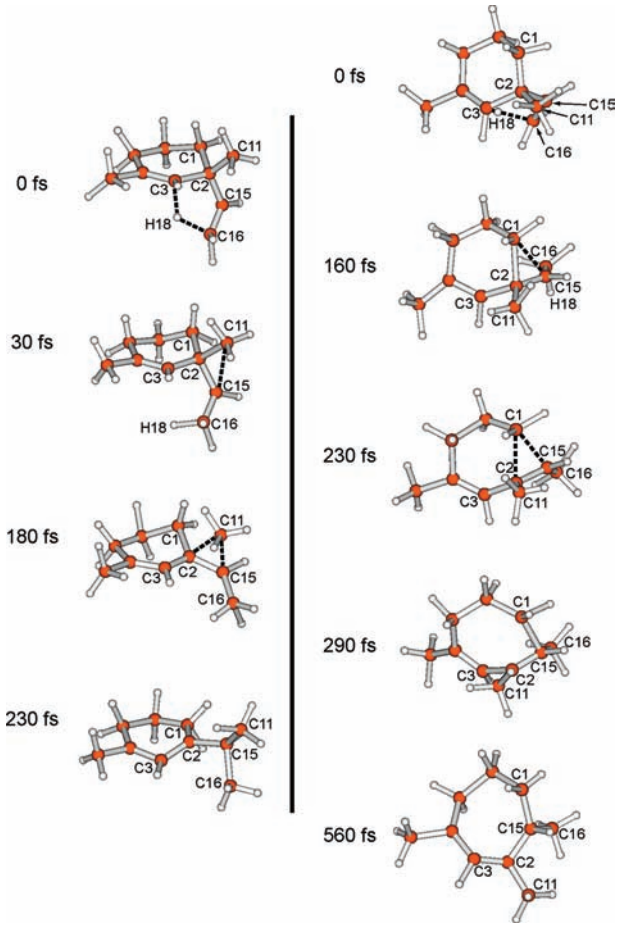

Figure 3. Snapshots of trajectories forming products **4** and **5** (left and right, respectively).

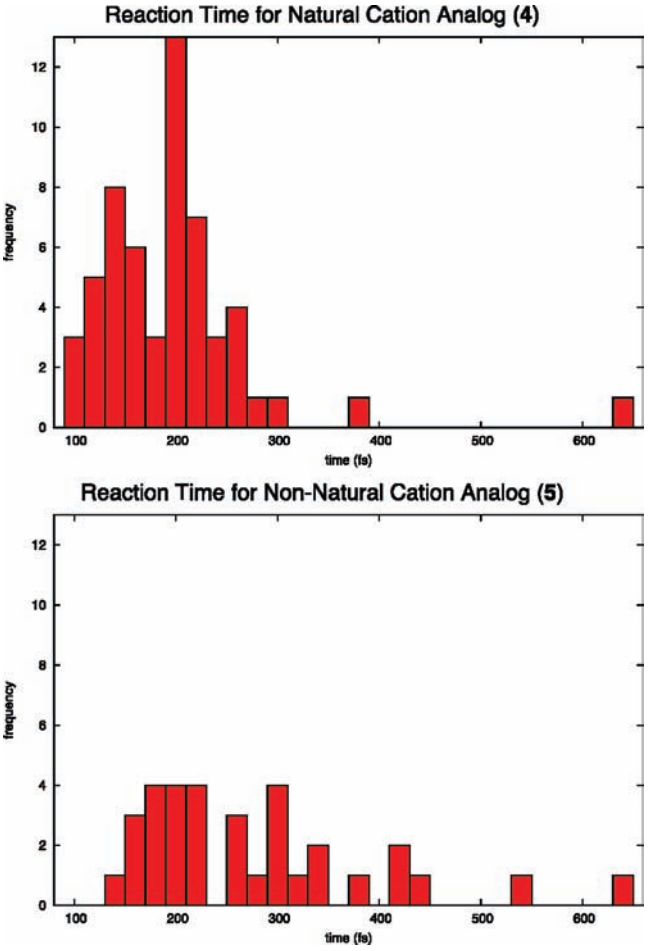

Figure 4. Distribution plots (histograms) for the amount of time for reaction to **4** (top) and **5** (bottom) to be completed.[37] Bin size is 20 fs.

the unoptimized Hessian integrator was 1.70 times that of the velocity Verlet for the same level of accuracy. Compared to the mean average total energy of 186.60 kcal/mol, the mean average energy variation for the velocity Verlet integrator after 1 ps is 0.74 kcal/mol. Integrating one trajectory for 1 ps took 1 week of computer time running on eight cores of a dual 2.66 GHz Xeon E5430 quad-core node.

To compare with the B3LYP/6-31+G(d,p) simulations, a smaller number of trajectories were calculated using MP2 with the same basis set and parameters as for the B3LYP trajectories. Each of these MP2 trajectories required 6 weeks of computer time running on the node described above.

Trajectory Initial Conditions and Ensembles. The direct dynamics trajectories were initiated at TS $\mathbf{2}^{\ddagger}$. The trajectory initial conditions were chosen from 330.15 K Boltzmann distributions for reaction coordinate translation, the vibrational degrees of freedom, and the three internal rotational degrees of freedom.[34] This model for initiating the trajectories assumes that recrossing of the TS is unimportant, so transition state theory (TST) gives an accurate rate constant for the $\mathbf{1} \rightarrow \mathbf{4} + \mathbf{5}$ reaction. The trajectories were directed off TS $\mathbf{2}^{\ddagger}$ toward the reaction products, and TS recrossing was found to be unimportant. Quasiclassical sampling, which includes ZPE, was used to randomly select vibrational states for the initial conditions. The normal-mode energies for the vibrational states were transformed to the Cartesian coordinates and velocities used for calculating the direct dynamics trajectories by choosing a random classical phase for each normal mode. Recent work[35] has shown that this approach for TS sampling leads to the same dynamics as using the Wigner distribution to transform the normal-mode energies to coordinates and momenta.

For the B3LYP/6-31+G(d,p) direct dynamics simulation, an ensemble of 100 trajectories was calculated. A similar ensemble of 21 trajectories was calculated for the MP2/6-31+G(d,p) direct dynamics.

RESULTS OF THE DIRECT DYNAMICS SIMULATIONS

Product Yield and Reaction Pathways. The results of the 100 direct dynamics trajectories calculated with B3LYP/6-31+G(d,p) are summarized in Figure 2. A very small fraction, only 5 out of 100, recross the TS and form the reactant, **1**. Of the remaining 95 trajectories, the majority (59%; 56 of 95 reactive events, $\sigma = 5$)[36] proceed to the analogue of abietadiene, **4**. Interestingly, we find that 35% (33 of 95 reactive events, $\sigma = 5$) of the reactive trajectories proceed to the analogue of the unobserved structure, **5**. On the basis of these dynamic simulations, the relative ratio of **4**:**5** is predicted to be 1.6:1 — a striking result, considering that the 20-carbon-atom product corresponding to **5** is not observed as a product of the enzyme-catalyzed process.[3]

All four pathways observed in the dynamics simulations have their first step in common: movement of the H-atom to form a methyl group at C16 (see Figure 2 for numbering). The distribution of products then diverges into one of two groups. The first group includes those products formed from alkyl group migration; **4** and **5** are included in this group. The second group involves more complex motions that cannot be considered alkyl group migrations; formation of **6** + **7** and **8** falls into this group.

dx.doi.org/10.1021/ja201730y |*J. Am. Chem. Soc.* 2011, 133, 8335–8343

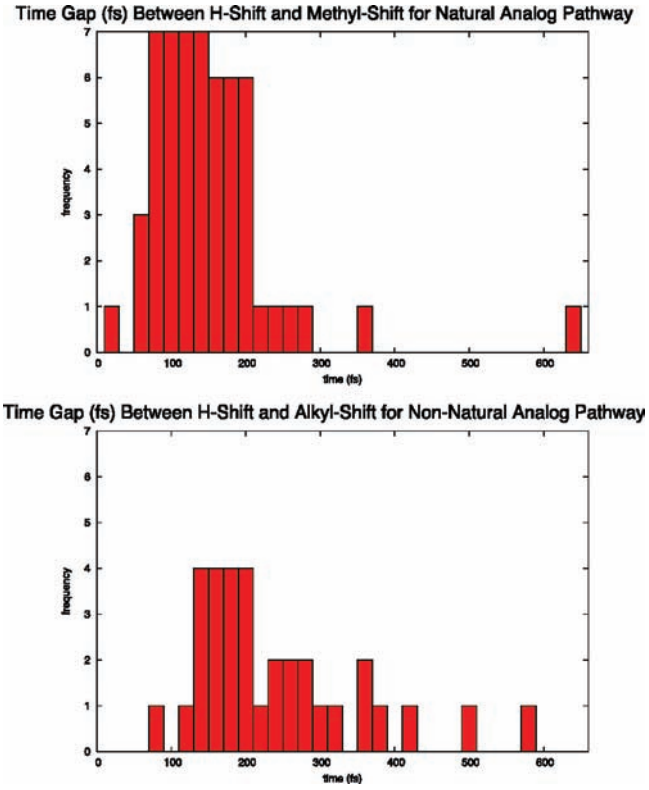

Figure 5. Distribution plots (histograms) for the time gap[38] between C−H and C−C bond-forming events[37] in the formation of **4** (top) and **5** (bottom). Bin size is 20 fs.

Atomic-Level Reaction Mechanisms. Figure 3 displays snapshots along example trajectories that form **4** and **5** (see Supporting Information for example movies). After the initial H-atom transfer, the formation of **4** occurs through a second event in which the methyl group, C11, shifts (breaking the C2−C11 bond and forming the C11−C15 bond). The 180 fs snapshot (Figure 3) provides a reasonable depiction of the TS for this requisite methyl shift. Overall this transformation into **4** happens quite quickly; on average H-transfer is complete by 44 fs (σ = 33 fs), while 191 fs (σ = 82 fs) delineates a complete process.[37]

Formation of **5** (Figure 3, right) is distinguished by a different alkyl shift than for the formation of **4** (here the C1−C2 bond breaks and a C1−C15 bond is formed). The 230 fs snapshot (Figure 3) provides a reasonable depiction of the TS for this alkyl shift. Overall transformation to **5** takes a bit longer than for formation of **4**. On average H-transfer is complete by 37 fs (σ = 24 fs), while 272 fs (σ = 115 fs) delineates a complete process.[37] For the example trajectories in Figure 3, relaxation to a structure resembling an equilibrium-geometry takes much longer for **5** (560 fs, cf. 230 fs for **4**). This difference in times is likely due to the fact that the equilibrium geometry of **5** is more dissimilar to the TS that precedes it than is the geometry of **4**. Figure 4 shows distribution plots (histograms) for the amount of time for the reaction to **4** (top) and **5** (bottom) to be completed.[37] Take note of the sharper shape of the distribution forming **4**. This is contrasted with the distribution forming **5**, which displays a wider spread. This difference in shape is also described by a longer average time for reaction completion (81 fs longer for **5** than for **4**) and a larger standard deviation in that time.

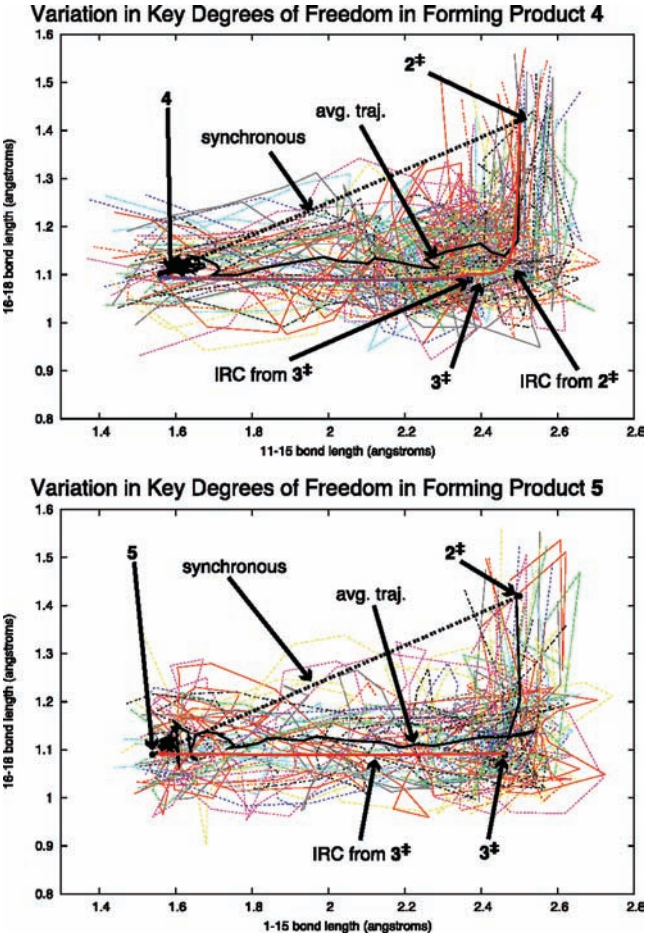

Figure 6. Plots of key pairs of reaction coordinates versus time for pathways forming **4** (top) and **5** (bottom). For each plot stationary points, the synchronous pathway, all trajectory data (truncated once the minimum is formed),[37] the average trajectory (black), and IRC path[5i] (red) are shown.

As a quantitative measure of how asynchronous the H- and C-shift events are in the formation of **4** and **5**, respectively, the time gap[38] (time between these events) was evaluated (see Figure 5 for distribution plots). Formation of **4** is accompanied by an average time gap of 147 fs (σ = 89 fs), while formation of **5** is accompanied by an average time gap of 235 fs (σ = 113 fs). To put this into perspective, the periodicity of C−C vibrations is ~42 fs, while that for C−H vibrations is ~11 fs,[39] meaning that approximately four to five C−C bond vibrations may occur between the C−H and C−C bond-forming events on the way to **4** and **5** — a substantial amount of time.

To further measure the asynchronous nature of the pathway forming **4** and **5**, primary reaction coordinates were chosen for each reaction: C11−C15 bond formation for **4**, C1−C15 bond formation for **5**, and C16−H18 bond formation for both pathways. The evolution of these reaction coordinates over the course of each trajectory is shown in Figure 6, where C11−C15 versus C16−H18 and C1−C15 versus C16−H18 are plotted versus time for formation of **4** and **5**, respectively.

For products **4** and **5**, Figure 6 shows that the average trajectory is highly asynchronous, evidenced by the fact that the C−H bond is formed entirely (vertical portions of average trajectories) before C−C bond formation. Furthermore, trajectories to **4** and **5** each

dx.doi.org/10.1021/ja201730y |J. Am. Chem. Soc. 2011, 133, 8335–8343

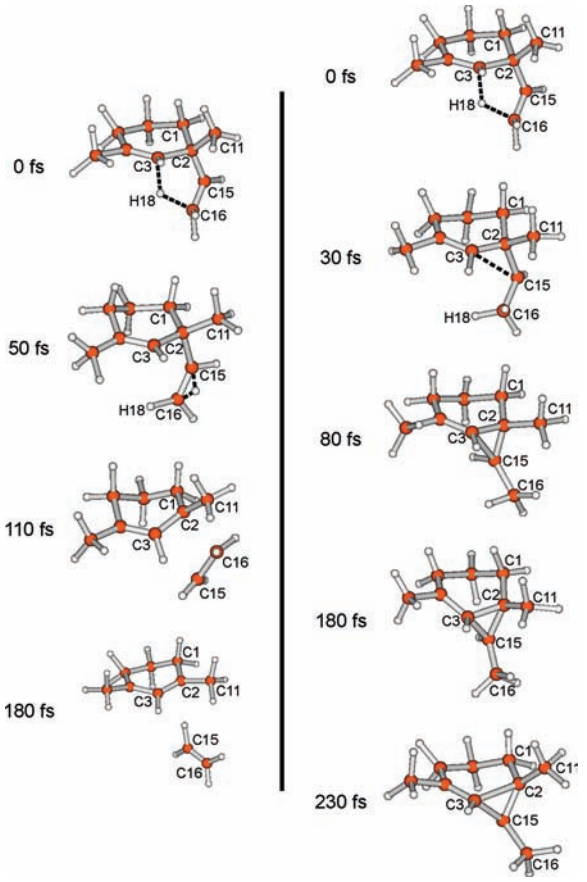

Figure 7. Snapshots of example trajectories forming products **6** + **7** and **8** (left and right, respectively).

follow (in an average manner) the IRC (minimum energy) pathway,[5i] as evidenced by a close correspondence between the IRC and average trajectory traces in Figure 6. It is important to note that often the atomic-level mechanism does not follow the IRC.[40]

We also observe other reactivity, namely elimination of ethylene (**6** + **7**, Figure 2) and an interesting cyclopropanation (**8**; see Figure 7 for snapshots from example trajectories). Elimination of ethylene takes place via a pair of tandem proton transfers. H18 is the proton transferring in $\mathbf{2}^{\ddagger}$, and this hydrogen atom is retained in the ethylene product. Once H18 has transferred, a second H transfer occurs, allowing for the elimination to occur. This elimination is a very fast process, with the initial H-shift completed by 10 fs and the secondary H-shift in progress by 50 fs. This is followed by C−C bond breakage that starts around 110 fs, and by 180 fs ethylene is well along its exit pathway. However, this reactivity is found in only a single reactive trajectory ($\sigma = 1$), making it a relatively low probability event.

The cyclopropanation forming **8** is distinguished from other pathways by the formation of a C3−C15 bond. **8** is approximately thermoneutral with respect to reactant **1**. Note that the thermal reaction of methyl cyclopropane, forming 1-butene is an analogue of this ring-opening (in reverse), which has been studied by others.[41] Formation of **8** occurs quite rapidly with the example trajectory (Figure 7, right) completed by 80 fs. On average (5 total events, $\sigma = 2$) H-transfer is complete by 54 fs ($\sigma = 38$ fs) while C−C bond formation occurs at 112 fs ($\sigma = 16$ fs).[37] At 58 fs ($\sigma = 46$ fs), the time gap for this process is substantially shorter than those for the production of **4** and **5**. In fact, the time gap is on the order of a single C−C bond vibration, which may classify it as a relatively synchronous reaction (with respect to the major C16−H18 and C3−C15 bond forming events). Also of interest are animations, which show that energy is heavily localized in the ring-fused C−C cyclopropane stretching mode (C2−C3); this is manifest in the snapshot at 230 fs, where the C−C bond is noticeably elongated (see Supporting Information for an example movie).

Comparison of B3LYP and MP2 Direct Dynamics. As a test of the validity of the B3LYP/6-31+G(d,p) trajectories, a smaller sample of MP2/6-31+G(d,p) trajectories was run. Due to the computational expense, substantially fewer MP2 trajectories were carried out (only 21; integrating one MP2 trajectory for 1 ps takes approximately 6 weeks of computational time on the nodes mentioned above — about 6 times as long as with B3LYP). Of these trajectories, 19 were found to be reactive, with 12 (63%) proceeding to abietadiene analogue **4** and 6 (32%) proceeding to non-natural analogue **5** (a ratio of 2:1 for **4**:**5**, cf. 1.6:1 from B3LYP results). Additionally, 1 reactive trajectory (5%) was found to proceed to the cyclopropanated compound **8**. These results are remarkably similar to those obtained with B3LYP, indicating an apparent insensitivity to model chemistry for this interesting reaction.

CONCLUSION

Our gas-phase dynamics simulations predict a relative product ratio for **4**:**5** of approximately 1.6:1. With the assumption that this model system (Scheme 3) mirrors that of its larger, 20-carbon congeners, this means that the enzyme abietadiene synthase must be steering this reaction to avoid the seven-membered ring containing product. Although there is an inherent dynamical preference for the observed natural product, it is not to the exclusion of detectable amounts of the alternative product. Possible means for steering the reaction toward the observed natural product include C−H/π[42] interactions, cation/π[43] interactions, and steric control. We plan to continue investigating this model system to pinpoint which factors dominate the abietadiene synthase reaction. We will also look to this model system to determine what role solvent might play in this interesting PES, with the potential for predicting what an experimental chemist might expect to see upon generation of **1** in the solution phase. Caution about whether this model system fails to capture all of the key dynamic effects cannot be overstated and will be addressed by trajectory simulations on the full 20-carbon system. Work is currently being carried out on all of these fronts, and we look forward to reporting on those results in the near future.

ASSOCIATED CONTENT

Supporting Information. Coordinates and energies for optimized structures and movies of select pathways. This material is available free of charge via the Internet at http://pubs.acs.org.

AUTHOR INFORMATION

Corresponding Author
bill.hase@ttu.edu

Present Addresses
[#]High Performance Computing Center, University of Arkansas, Fayetteville, AR 72701

■ ACKNOWLEDGMENT

This material is based upon work supported by the National Science Foundation under Grant Nos. CHE-0957521 and CHE-0957416 and the Robert A. Welch Foundation under Grant No. D-0005. Support was also provided by the High Performance Computing Center (HPCC) at Texas Tech University, under the direction of Philip W. Smith, as well as the Texas Advanced Computing Center (TACC) of the University of Texas at Austin. Further, we thank R. M. Shroll (Spectral Sciences, Inc.), W. A. deJong (Pacific Northwest National Laboratories), Kyoyeon Park (Texas Tech University), and Young Hong (UC Davis) for helpful comments.

■ REFERENCES

(1) Phillips, M. A.; Croteau, R. B. *Trends Plant Sci.* **1999**, *4*, 184–190.
(2) McCoy, M. *Chem. Eng. News* **2000**, *78*, 13–15.
(3) (a) LaFever, R. E.; Stofer Vogel, B.; Croteau, R. *Arch. Biochem. Biophys.* **1994**, *313*, 139–149. (b) Peters, R. J.; Flory, J. E.; Jetter, R.; Ravn, M. M.; Lee, H.-J.; Coates, R. M.; Croteau, R. B. *Biochemistry* **2000**, *39*, 15592–15602. (c) Peters, R. J.; Croteau, R. B. *Proc. Natl. Acad. Sci. U.S.A.* **2002**, *99*, 580–584. (d) Peters, R. J.; Ravn, M. M.; Coates, R. M.; Croteau, R. B. *J. Am. Chem. Soc.* **2001**, *123*, 8974–8978. (e) Funk, C.; Croteau, R. *Arch. Biochem. Biophys.* **1994**, *308*, 258–266. (f) Ravn, M. M.; Coates, R. M.; Jetter, R.; Croteau, R. B. *Chem. Commun.* **1998**, 21–22. (g) Ravn, M. M.; Coates, R. M.; Flory, J. E.; Peters, R. J.; Croteau, R. *Org. Lett.* **2000**, *2*, 573–576. (h) Ravn, M. M.; Peters, R. J.; Coates, R. M.; Croteau, R. *J. Am. Chem. Soc.* **2002**, *124*, 6998–7006. (i) Wilderman, P. R.; Peters, R. J. *J. Am. Chem. Soc.* **2007**, *129*, 15736–15737.
(4) Numbering of abietic acid adopted from ref 3a.
(5) (a) Hong, Y. J.; Tantillo, D. J. *J. Am. Chem. Soc.* **2009**, *131*, 7999–8015. (b) Ho, G. A.; Nouri, D. H.; Tantillo, D. J. *Tetrahedron Lett.* **2009**, *50*, 1578–1584. (c) Wang, S. C.; Tantillo, D. J. *Org. Lett.* **2008**, *10*, 4827–4830. (d) Lodewyk, M. W.; Gutta, P.; Tantillo, D. J. *J. Org. Chem.* **2008**, *73*, 6570–6579. (e) Gutta, P.; Tantillo, D. J. *Org. Lett.* **2007**, *9*, 1069–1071. (f) Hong, Y. J.; Tantillo, D. J. *Org. Lett.* **2006**, *8*, 4601–4604. (g) Gutta, P.; Tantillo, D. J. *J. Am. Chem. Soc.* **2006**, *128*, 6172–6179. (h) Ho, G. A.; Nouri, D. H.; Tantillo, D. J. *J. Org. Chem.* **2005**, *70*, 5139–5143. (i) Hong, Y. J.; Tantillo, D. J. *Nature Chem.* **2009**, *1*, 384–389. (j) Tantillo, D. J. *Chem. Soc. Rev.* **2010**, *39*, 2847–2854.
(6) (a) Christianson, D. W. *Curr. Opin. Chem. Biol.* **2008**, *12*, 141–150. (b) Christianson, D. W. *Chem. Rev.* **2006**, *106*, 3412–3442. (c) Davis, E. M.; Croteau, R. *Top. Curr. Chem.* **2000**, *209*, 53–95. (d) Cane, D. E. *Chem. Rev.* **1990**, *90*, 1089–1103.
(7) (a) Tantillo, D. J. *J. Phys. Org. Chem.* **2008**, *21*, 561–570. The term "two-stage" has also been proposed to describe a reaction that takes place in a single kinetic step but with asynchronous events: (b) Dewar, M. J. S. *J. Am. Chem. Soc.* **1984**, *106*, 209–219.
(8) Ess, D. H.; Wheeler, S. E.; Iafe, R. G.; Xu, L.; Çelebi-Ölçüm, N.; Houk, K. N. *Angew. Chem., Int. Ed.* **2008**, *47*, 7592–7601.
(9) (a) Ramquet, M.-N.; Dive, G.; Dehareng, D. *J. Chem. Phys.* **2000**, *112*, 4923–4934. (b) Valtazanos, P.; Ruedenberg, K. *Theor. Chim. Acta* **1986**, *69*, 281–307.
(10) Lourderaj, U.; Park, K.; Hase, W. L. *Int. J. Phys. Chem.* **2008**, *27*, 361–403.
(11) (a) Thomas, J. B.; Waas, J. R.; Harmata, M.; Singleton, D. A. *J. Am. Chem. Soc.* **2008**, *130*, 14544–14555. (b) Hamaguchi, M.; Nakishi, M.; Nagai, T.; Nakamura, T.; Abe, M. *J. Am. Chem. Soc.* **2007**, *129*, 12981–12988. (c) Singleton, D. A.; Hang, C.; Szymanski, M. J.; Meyer, M. P.; Leach, A. G.; Kuwata, K. T.; Chen, J. S.; Greer, A.; Foote, C. S.; Houk, K. N. *J. Am. Chem. Soc.* **2003**, *125*, 1319–1328. (d) Wales, D. J. *J. Chem. Phys.* **2000**, *113*, 3926–3927.
(12) Williams, T.; Kelley, C. *GNUPlot 4.0.0*; broeker, 2004.
(13) (a) Sun, L.; Hase, W. L. *Rev. Comput. Chem.* **2003**, *19*, 79–146. (b) Bolton, K.; Hase, W. L.; Peslherbe, G. H. . In *Multidimensional Molecular Dynamics Methods*; Thompson, D. L., Ed.; World Scientific Publishing, Inc.: London, 1998; pp 143−189.
(14) (a) Bylaska, E. J.; de Jong, W. A.; Govind, N.; Kowalski, K.; Straatsma, T. P.; Valiev, M.; Wang, D.; Apra, E.; Windus, T. L.; Hammond, J.; Nichols, P.; *NWChem*, A Computational Chemistry Package for Parallel Computers, Version 5.1; Pacific Northwest National Laboratory: Richland, WA, 2007. (b) Kendall, R. A.; Apra, E.; Bernholdt, D. E.; Bylaska, E. J.; Dupuis, M.; Fann, G. I.; Harrison, R. J.; Ju, J.; Nichols, J. A.; Nieplocha, J.; Straatsma, T. P.; Windus, T. L.; Wong, A. T. *Comput. Phys. Commun.* **2000**, *128*, 260–283.
(15) Møller, C.; Plesset, M. S. *Phys. Rev.* **1934**, *46*, 618–622.
(16) (a) Becke, A. D. *J. Chem. Phys.* **1993**, *98*, 5648–5652. (b) Becke, A. D. *J. Chem. Phys.* **1993**, *98*, 1372–1377. (c) Lee, C.; Yang, W.; Parr, R. G. *Phys. Rev. B: Solid State* **1988**, *37*, 785–789. (d) Stevens, P. J.; Devlin, F. J.; Chabalowski, C. F.; Frisch, M. J. *J. Phys. Chem.* **1994**, *98*, 11623–11627.
(17) Zhao, Y.; Lynch, B. J.; Truhlar, D. G. *J. Phys. Chem. A* **2004**, *108*, 2715–2719.
(18) Zhao, Y.; Schultz, N. E.; Truhlar, D. G. *J. Chem. Theory Comput.* **2006**, *2*, 364–382.
(19) The 6-31+G(d,p) basis set is not standard in NWChem; it was generated as a composite of the 6-31G(d,p) and the diffuse function from 6-31+G(d) as acquired from the EMSL basis set exchange: (a) Schuchardt, K. L.; Didler, B. T.; Elsethagen, T.; Sun, L.; Gurumoorthi, V.; Chase, J.; Li, J.; Windus, T. L. *J. Chem. Inf. Model.* **2007**, *47*, 1045–1052. (b) Feller, D. *J. Comput. Chem.* **1996**, *17*, 1571–1586. Explicit basis set specifications used for the calculations herein can be found in the Supporting Information.
(20) Dunning, T. H., Jr. *J. Chem. Phys.* **1989**, *90*, 1007–1023.
(21) (a) Wheeler, S. E.; Houk, K. N. *J. Chem. Theory Comput* **2010**, *6*, 395–404. (b) Tirado-Rives, J.; Jergensen, W. L. *J. Chem. Theory Comput.* **2008**, *4*, 297–306. (c) Zhang, J.; Zhao, Y.; Truhlar, D. G. *J. Chem. Theory Comput.* **2007**, *3*, 569–582. (d) Riley, K. E.; Op't Holt, B. T.; Merz, K. M., Jr. *J. Chem. Theory Comput.* **2007**, *3*, 407–433. (e) Lynch, B. J.; Truhlar, D. G. *J. Phys. Chem. A* **2003**, *107*, 8996–8999. (f) Curtiss, L. A.; Raghavachari, K.; Redfern, P. C.; Pople, J. A. *J. Chem. Phys.* **2000**, *112*, 7374–7383. (g) Curtiss, L. A.; Raghavachari, K.; Redfern, P. C.; Pople, J. A. *J. Chem. Phys.* **1997**, *106*, 1063–1079. For comparisons in terpene related carbocations, see, for example: (h) Hong, Y. J.; Tantillo, D. J. *Org. Biomol. Chem.* **2010**, *8*, 4589–4600. (i) Weitman, M.; Major, D. T. *J. Am. Chem. Soc.* **2010**, *132*, 6349–6360.
(22) Raghavachari, K.; Trucks, G. W.; Pople, J. A.; Head-Gordon, M. *Chem. Phys. Lett.* **1989**, *157*, 479–483.
(23) Woodcock, H. L.; Schaefer, H. F.; Schreiner, P. R. *J. Phys. Chem. A* **2002**, *106*, 11923–11931.
(24) Tsuzuki, S.; Lüthi, H. P. *J. Chem. Phys.* **2001**, *114*, 3949–3957.
(25) (a) Schreiner, P. R.; Fokin, A. A.; Pascal, R. A., Jr.; de Meijera, A. *Org. Lett.* **2006**, *8*, 3635–3638. (b) Check, C. E.; Gilbert, T. M. *J. Org. Chem.* **2005**, *70*, 9828–9834. (c) Redfern, P. C.; Zapol, P.; Curtiss, L. A.; Raghavachari, K. *J. Phys. Chem. A* **2000**, *104*, 5850–5854.
(26) (a) Wodrich, M. D.; Wannere, C. S.; Mp, Y.; Jarowski, P. D.; Houk, K. N.; Schleyer, P. v. R. *Chem.—Eur. J.* **2007**, *13*, 7731–7744. (b) Grimme, S. *Angew. Chem., Int. Ed.* **2006**, *45*, 4460–4464. (c) Wodrich, M. D.; Corminboeuf, C.; Schleyer, P. v. R. *Org. Lett.* **2006**, *8*, 3631–3634.
(27) For a good overview of the problems associated with B3LYP, see: (a) Kang, J. K.; Musgrave, C. B. *J. Chem. Phys.* **2001**, *115*, 11040–11051. For a report suggesting that B3LYP tends to underestimate reaction barriers and overestimate reaction thermochemistry, see: (b) Lynch, B. J.; Fast, P. L.; Harris, M.; Truhlar, D. G. *J. Phys. Chem. A* **2000**, *104*, 4811–4815. For reports that indicate B3LYP underestimates the strength of hydrogen bonds, see ref 24 and (c) Zhao, Y.; Tishchenko, O.; Truhlar, D. G. *J. Phys. Chem. B* **2005**, *109*, 19046–19051.
(28) (a) Zheng, J.; Zhao, Y.; Truhlar, D. G. *J. Chem. Theory Comput.* **2007**, *3*, 569–582. (b) Zhao, Y.; Schultz, N. E.; Truhlar, D. G. *J. Chem. Theory Comput.* **2006**, *2*, 364–382. (c) Zhao, Y.; Lynch, B. J.; Truhlar, D. G. *J. Phys. Chem. A* **2004**, *108*, 2715–2719. (d) Lynch, B. J.; Truhlar, D. G. *J. Phys. Chem. A* **2003**, *107*, 8996–8999.

(29) (a) Siebert, M. R.; Tantillo, D. J. *J. Phys. Org. Chem.* **2007**, *20*, 384–394. (b) Siebert, M. R.; Tantillo, D. J. *J. Org. Chem.* **2006**, *71*, 645–654. (c) Vrcek, I. V.; Vrcek, V.; Siehl, H.-U. *J. Phys. Chem. A* **2002**, *106*, 1604–1611. (d) Farcasiu, D.; Lukinskas, P.; Pamidighantam, S. V. *J. Phys. Chem. A* **2002**, *106*, 11672–11675.

(30) (a) Hase, W. L.; Bolton, K.; Sainte Claire, P. d.; Duchovic, R. J.; Hu, X.; Komornicki, A.; Li, G.; Lim, K. F.; Lu, D.-h.; Peslherbe, G. H.; Song, K.; Swamy, K. N.; Vande Linde, S. R.; Varandas, A.; Wang, H.; Wolf, R. J. *Venus05*, a general chemical dynamics computer program; 2004. (b) Hase, W. L.; Duchovic, R. J.; Hu, X.; Komornicki, A.; Lim, K. F.; Lu, D. H.; Peslherbe, G. H.; Swamy, S. R.; Vande Linde, S. R.; Varandas, A.; Wang, H.; Wolf, R. J. *QCPE Bull.* **1996**, *16*, 671. (c) Hu, X.; Hase, W. L.; Pirraglia, T. *J. Comput. Chem.* **1991**, *12*, 1014–1024.

(31) Swope, W. C.; Anderson, H. C.; Berens, P. H.; Wilson, K. R. *J. Chem. Phys.* **1982**, *76*, 637–649.

(32) (a) Schlier, C.; Seiter, A. *Comput. Phys. Commun.* **2000**, *130*, 176–189. (b) Schlier, C.; Seiter, A. *J. Phys. Chem. A* **1998**, *102*, 9399–9404.

(33) Lourderaj, U.; Song, K.; Windus, T. L.; Zhuang, Y.; Hase, W. L. *J. Chem. Phys.* **2007**, *126*, 044105.

(34) Peslherbe, G. H.; Wang, H.; Hase, W. L. *Adv. Chem. Phys.* **1999**, *105*, 171–201.

(35) Sun, L.; Hase, W. L. *J. Chem. Phys.* **2010**, *133*, 034027.

(36) Truhlar, D. G.; Muckerman, J. T. In *Atom-Molecule Collision Theory: A Guide fort he Experimentalist*; Bernstein, R. B., Ed.; Plenum: New York, 1979; pp 505−566.

(37) Each event was deemed complete at the first time that the interatomic distance in question fell below the distance for the equilibrium structure. For **4**, key equilibrium interatomic distances are 1.10 and 1.56 Å for the C16−H18 and C11−C15 bonds, respectively; for **5**, these distances are 1.09 and 1.54 Å for the C16−H18 and C1−C15 bonds, respectively; and for **8**, these distances are 1.10 and 1.59 Å for the C16−H18 and C3−C15 bonds, respectively. Interatomic distances were printed every 10 fs, which represents the resolution in which the stated times reside.

(38) Xu, L.; Doubleday, C. E.; Houk, K. N. *J. Am. Chem. Soc.* **2010**, *132*, 3029–3037.

(39) The vibrational modes for **4** were visually inspected. The C16−H18 stretch (the C−H bond formed in the reaction) appears at 3059 cm^{-1}, and the C11−C15 stretch (the C−C bond formed in the generation of **4**) is best represented by a stretch at 795 cm^{-1}; these frequencies correspond to 11 and 42 fs, respectively.

(40) (a) López, J. G.; Vayner, G.; Lourderaj, U.; Addepalli, S. V.; Kato, S.; de Jong, W. A.; Windus, T. L.; Hase, W. L. *J. Am. Chem. Soc.* **2007**, *129*, 9976–9985. (b) Sun, L.; Song, K.; Hase, W. L. *Science* **2002**, *296*, 875–878. (c) Mann, D. J.; Hase, W. L. *J. Am. Chem. Soc.* **2002**, *124*, 3208–3209.

(41) (a) Goodrow, A.; Bell, A. T.; Head-Gordon, M. *J. Chem. Phys.* **2009**, *130*, 244108. (b) Kalra, B. L.; Cho, J. Y.; Lewis, D. K. *J. Phys. Chem. A* **1999**, *103*, 362–364. (c) Setser, D. W.; Rabinovitch, B. S. *J. Am. Chem. Soc.* **1964**, *86*, 564–569. (d) Chesick, J. P. *J. Am. Chem. Soc.* **1960**, *82*, 3277–3285.

(42) (a) Nishio, M.; Hirota, M.; Umezawa, Y. *The CH/π Interaction: Evidence, Nature, and Consequences*; Wiley-VCH: New York, 1998. (b) Brandl, M.; Weiss, M. S.; Jabs, A.; Sühnel, J.; Hilgenfeld, R. *J. Mol. Biol.* **2001**, *307*, 357–377. (c) Tsuzuki, S.; Honda, K.; Uchimaru, T.; Mikami, M.; Tanabe, K. *J. Am. Chem. Soc.* **2000**, *122*, 3746–3753.

(43) (a) Ma., J. C.; Dougherty, D. A. *Chem. Rev.* **1997**, *97*, 1303–1324. (b) Dougherty, D. A. *Science* **1996**, *271*, 163–168. (c) Hong, Y. J.; Tantillo, D. J. *J. Org. Chem.* **2007**, *72*, 8877–8881.